Polymorphous Structures and Their Phase Relationships in a Main-Chain/Side-Chain Liquid Crystalline Polyester

Jrjeng Ruan, Jason J. Ge, Anqiu Zhang, Jin Shi, Shy-Yeu Wang, Frank W. Harris, and Stephen Z. D. Cheng*

Maurice Morton Institute and Department of Polymer Science, The University of Akron, Akron, Ohio 44325-3909

Received September 4, 2001; Revised Manuscript Received November 8, 2001

ABSTRACT: A series of specially designed polyesters consisting of aromatic main-chain/side-chain liquid crystalline (LC) polymers for flat-panel display applications have been synthesized via polycondensation of 2,2′-bis(trifluoromethyl)-4,4′-biphenyldicarbonyl chloride with 2,2′-bis{ω-[4-(4-cyanophenyl) phenyoxy]-*n*-alkoxycarbonyl}-4,4′-biphenyldiol (PEFBP(*n*), where *n* is the number of methylene units in the side chains). For a PEFBP polyester of which a 4-cyanobiphenyl mesogen in each side chain is coupled with the aromatic backbone via seven methylene units, PEFBP(*n*=7), complicated polymorphism has been identified during its structural evolutions. On the basis of differential scanning calorimetry, wide-angle X-ray diffraction, electron diffraction (ED), polarized light, and transmission electron microscopy (TEM) experiments, it is found that this polymer possesses three triclinic crystalline (K_{t1}, K_{t2}, and K_{t3}) phases having the same symmetry but different unit cell dimensions, one highly ordered LC smectic phase having an orthorhombic (SK_O) structure, and one nematic (N) phase. Both of the triclinic K_{t1} and K_{t3} structures are also confirmed by the ED results. Investigations of thermodynamic phase stability relationships indicate that when PEFBP(*n*=7) is crystallized from the N phase, the K_{t1} phase forms. During heating, this K_{t1} phase transfers to the K_{t3} phase via reorganization and melting/recrystallization before it enters the N phase. However, when the sample is first cooled to below 130 °C to form the SK_O phase, the K_{t2} phase develops during heating. Further heating the K_{t2} phase leads to a transformation to the K_{t3} phase at high temperatures via, again, reorganization and melting/recrystallization. Nevertheless, no apparent transformation between the K_{t1} and K_{t2} phases is experimentally observed. Polarized infrared spectroscopy experimental results indicate that the aromatic polyester backbones and 4-cyanobiphenyl mesogens are parallel to each other and packed into one crystal unit cell. TEM observations show different morphological characteristics of the K_{t1} and K_{t3} phases. It is concluded that the K_{t3} phase is the thermodynamically most stable phase, and the K_{t1} and K_{t2} phases are metastable. These two phases can be experimentally accessed only because the crystallization rate of the K_{t3} phase is much slower than those of the K_{t1} and K_{t2} phases.

Introduction

Among the various new developments in polymer materials, the design and investigation of liquid crystalline polymers (LCPs) have been one of the most growing activities for their distinctive roles in biomimetic behaviors and electrooptical applications. Molecular architecture of LCPs emerges to be one of important elements in achieving desired physical properties via soft-ordered structural formations. Among different structural designs in LCPs, one interesting approach is to introduce flexible side chains onto the rigid-rodlike backbones in polymers.[1−5] It has also been reported that in these comb-shaped LCPs mesogens can also be incorporated into the side chains.[6−9] Consequently, the characteristics of chemical structures of the main-chain and side-chain mesogens, such as azobenzene and azoxybenzene,[10−15] *p*-phenylene benzoate,[14,16] and biphenylene,[15−17] may influence the molecular packing, the order of mesophases, and sometimes even the formation of nanoscale suprastructures.

The structural order of the main-chain LCPs with flexible side chains have been believed to be board- or ribbonlike,[18−20] while other structures are also reported.[21] Their backbones are usually composed of aromatic polyamides, polyesters, or polyimides, with attached long pendant side chains (of which most of the cases are methylene units). The entire macromolecules are packed in layers partially due to the molecular architecture and immiscibility of the backbones and side chains. This leads to multiple molecular relaxation processes and complicated polymorphism observed in these LC polymers.[22−27] An advanced review of combined LC main-chain/side-chain polymers can be found in ref 28.

Recently, a series of specifically designed polyesters with 4-cyanobiphenyl mesogens coupled with different number of methylene units in the side chains have been synthesized. The purpose of synthesizing this series of polymers is due to their specific behavior in forming alignment layers with very high and stable pretilt angles (ϕ > 30°) via mechanical rubbing in flat-panel display applications.[29−31] Furthermore, it has also been found that the high pretilt angle is surprisingly oriented against the rubbing direction to possess a negative angle ($-\phi$) due to the side-chain conformational rearrangement during the rubbing.[30,31] The general chemical structure of these compounds is

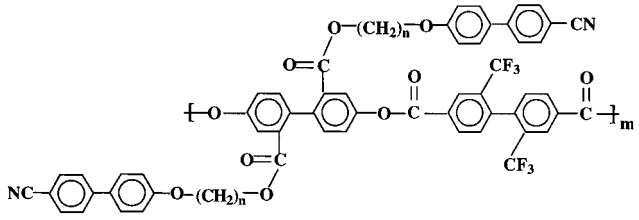

* To whom correspondence should be addressed. E-mail: cheng@polymer.uakron.edu.

10.1021/ma0115702 CCC: $22.00
Published on Web 12/18/2001

To further understand the molecular packing in LC and crystalline phases and their phase relationships of this series of PEFBPs(n), we have carried out a systematic study on phase structures and transformations of PEFBPs(n = 8, 9, 10, and 11). It has been found that phase behaviors of this series of polymers exhibit an interesting odd−even effect. PEFBPs(n = even) only possess LC phases, while for PEFBPs(n = odd) both LC and crystalline polymorphism have been identified.[8,9] Here, we report polymorphous structures and their phase relationships on one of this PEFBP series, of which a 4-cyanobiphenyl mesogen in each side chain is coupled with the aromatic backbone via seven methylene units, PEFBP(n = 7). Compared with those previous studies,[8,9] this polymer is the most difficult one to study since the methylene unit number in the side chains is the smallest. This results in not only a higher glass transition temperature (T_g) and other transition temperatures but also a change of the coupling power between the 4-cyanobiphenyls and the backbones. This may lead to complicated phase transformation behaviors and substantially reduce the molecular dynamics and thus crystallization rates, while monotropic metastable phases may also appear in PEFBP(n = 7).

Experimental Section

Materials and Samples. The synthesis of this series of PEFBPs(n) LC polyesters was report previously via a polycondensation of 2,2′-bis(trifluoromethyl)-4,4′-biphenyldicarbonyl chloride with 2,2′-bis{ω-[4-(4-cyanophenyl)phenyoxy]-n-alkoxycarbonyl]}-4,4′-biphenyldiol (PEFBP).[32] The polymer was further fractionated using a chloroform/methanol mixed solvent. A relative number molecular weight of this polymer was determined to be 18 000 g/mol by gel permeation chromatography based on the polystyrene standard, and the polydispersity was 1.6. The polymer was dried in a vacuum oven overnight all the time before being used.

PEFBP(n = 7) powder samples were used in differential scanning calorimetric (DSC) and one-dimensional (1D) wide-angle X-ray diffraction (WAXD) studies. Fibers were spun at 175 °C from the LC phase for structural determinations in 2D WAXD experiments. The fiber diameter was around 30 μm. Samples prepared for polarized Fourier transform infrared (IR) spectroscopy experiments were sheared uniaxially at 175 °C on the surface of KBr and then quenched to room temperature. To obtain different crystal structures, the samples were isothermally kept at different crystallization temperature (T_c) between 130 and 205 °C for various periods of time (t_c). Solution-casting thin films with thickness less than 0.3 μm were prepared from 0.25% (w/w) solution in THF for transmission electron microscopy (TEM) studies. In polarized light microscopy (PLM) experiments, the films with a thickness of ~10 μm were obtained via the melt-casting procedure. Microscopic samples' thermal histories were identical to those DSC, WAXD, and IR experiments.

Equipment and Experiments. DSC experiments were performed on a Perkin-Elmer DSC-7. The temperature and heat flow scales were calibrated using standard materials at different cooling and heating rates (between 2.5 and 40 °C/min). The transition temperature of the LC phase was determined using an on-set temperature, which was defined by the cross point of the peak slope and the baseline in DSC thermal diagrams. In cooling, the on-set temperature was determined on the high-temperature side, and upon heating this temperature was on the low-temperature side. Isothermal experiments were also carried out to study the phase structures. The samples were first heated to 245 °C and kept in the nematic (N) state for 2 min instead of in the isotropic melt (I) in order to avoid sample degradation. They were then quenched to preset T_c and held there for different periods of t_c to allow crystallization. The samples were subsequently quenched to room temperature, which was below the T_g. Heating experiments to the isotropic temperature (T_i) at 10 °C/min were then recorded.

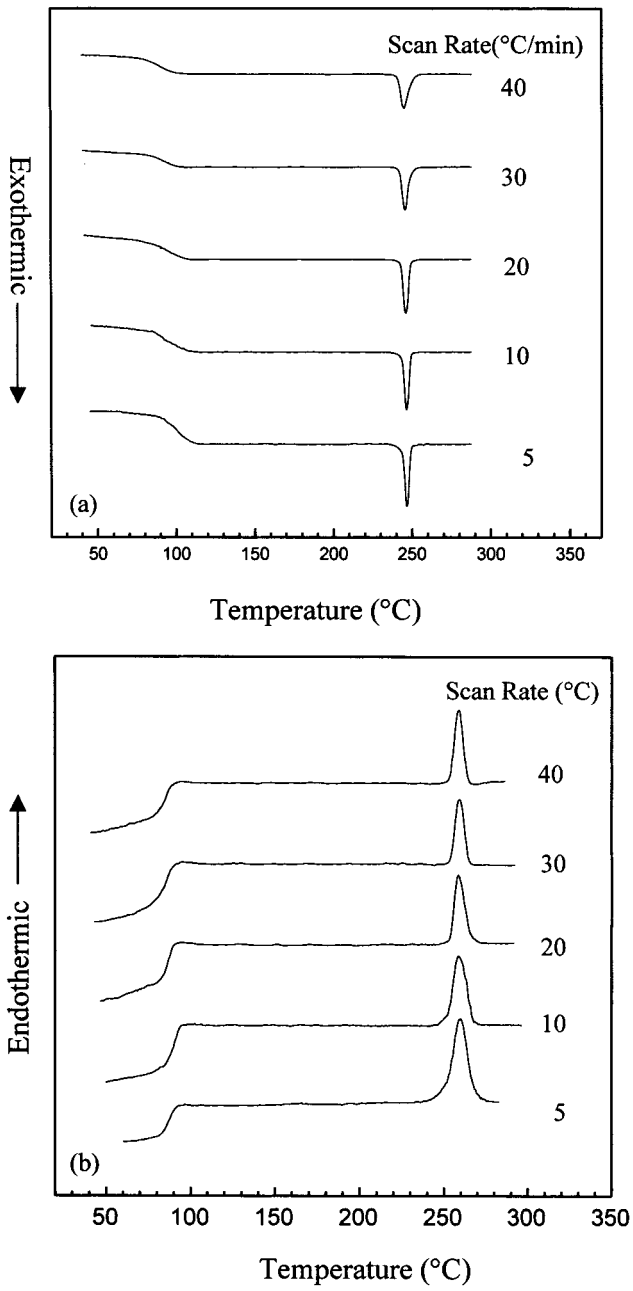

Figure 1. Two sets of DSC cooling (a) and subsequently heating (b) diagrams for the samples at different rates.

Phase structures and transformations were recognized using 1D WAXD experiments, and they were carried out using a diffractometer on a Rigaku 12 kW rotating-anode generator (Cu Kα) coupled with a hot stage. When the isothermal experiments were conducted, the 1D WAXD patterns were recorded at a scan rate 0.5°/min. For the time-resolve heating and cooling experiments, the WAXD scanning rate was 7°/min. To identify different phase structures, 2D WAXD fiber experiments were conducted on a Rigaku 18 kW rotating-anode generator (Cu Kα) equipped an image plate with a hot stage. Espousal times of the fiber patterns were controlled within hours. Both of the X-ray beams were monochromatized using graphite crystals. The reflection peak positions and widths observed on the powder and fiber patterns were calibrated with silicon crystals for known 2θ diffractions and crystallite sizes when 2θ > 15° and with silver behenate for 2θ < 15°. The deviation of measuring diffraction angle was ±0.05°. The

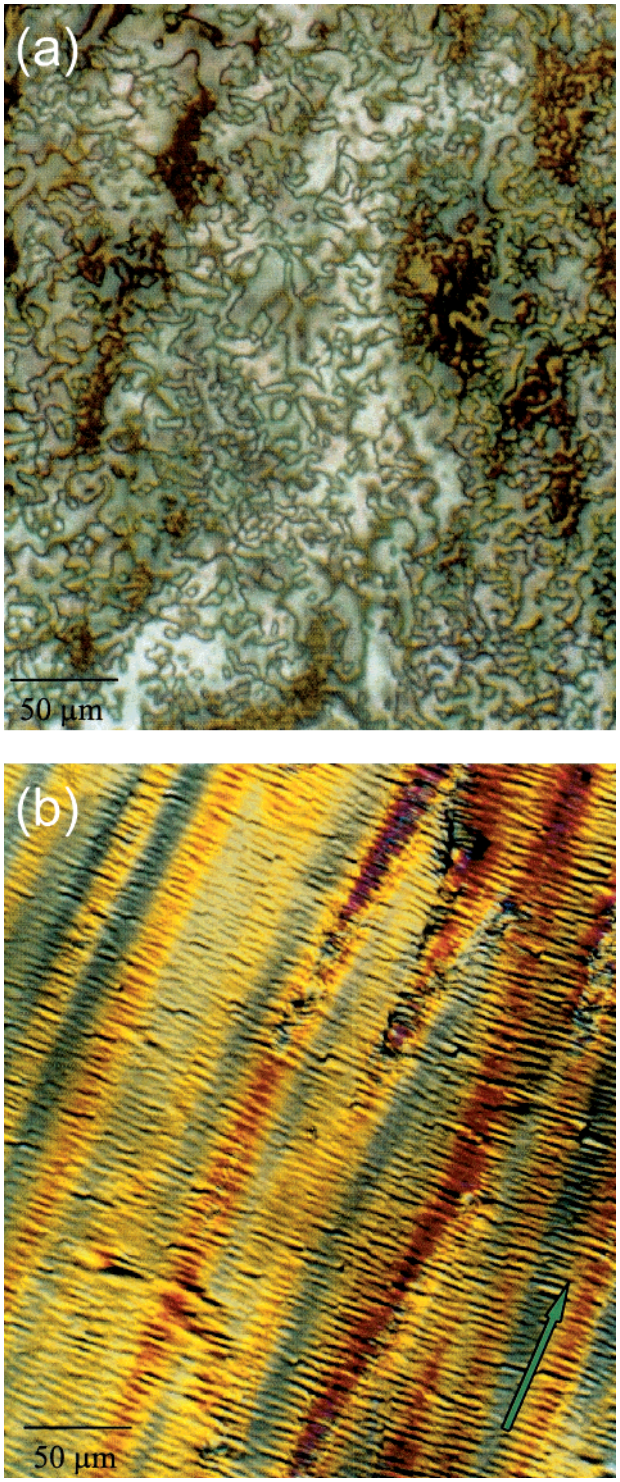

Figure 2. PLM liquid LC schlieren texture observed after the sample was isothermally kept at 120 °C for 12 h.

crystal unit-cell determination procedure was based on construction of the reciprocal lattice. Computer refinement was conducted to find the solutions with the least error between calculation values and experimental results.[33,34]

Polarized IR spectroscopy (Mattson Galaxy series FT-IR 5000) experiments were carried out in a transmission mode with a He:neon laser source and a polarizer rotation stage having the rotation angle ranged from 0° to 90° (the accuracy of ±0.5° in the azimuthal direction). The accuracy of the wavenumber was within 4 cm^{-1}. The calculation of dichroic ratio ($A_{\parallel}/A_{\perp}$) was carried out using the ratio of the intensity obtained between the parallel (0°) and the perpendicular (90°) spectra with respect to the orientation direction.

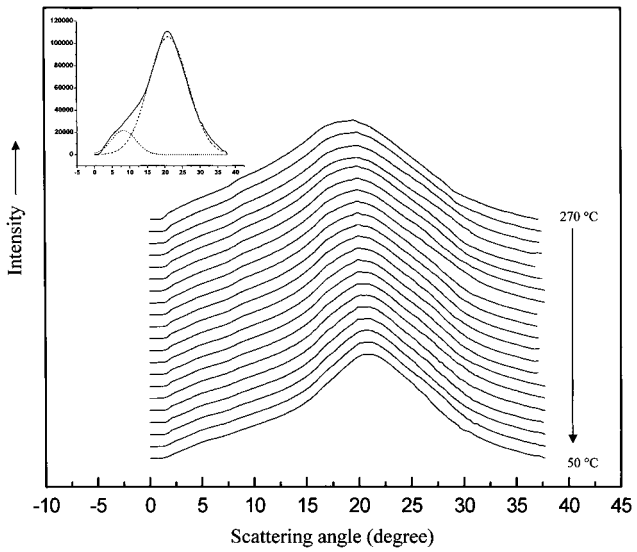

Figure 3. Set of WAXD powder pattern at different temperatures after the sample was quenched from the isotropic melt to below its T_g. Deconvolutions are also included in this figure.

Morphological observation of the N phase on a micrometer scale was conducted on an Olympus(HB-2) PLM coupled with a Mettler hot stage FP-91, while a JEOL (1200 EX II) TEM was used to study crystal morphology on a nanometer scale. Selected area electron diffraction (SAED) experiments were also carried out in TEM (the accelerating voltage was 120 kV). The TEM samples were deposited on carbon-coated glass surface and shadowed by Pt for better contrast. The samples were then detached from the glass surface and picked up on the Cu grids. To obtain different zones in the SAED, a tilting stage was also used. Calibration of the ED spacing was conducted by using TlCl and Au.

Results and Discussion

Identification of the Low-Ordered LC Phases. Figure 1a,b shows two sets of DSC cooling and subsequent heating diagrams for PEFBP(n = 7) at different rates (between 5 and 40 °C/min). A T_g at 88 °C and an on-set first-order transition temperature at 255 °C can be observed. The first-order transition temperature and its heat of transition (2.78 kJ/mol) remain invariant upon the cooling and heating rates. The samples have also been isothermally kept at T_c = 120 or 130 °C for 16 h after being quenched from the N phase; no new exothermic and endothermic events can be found during heating these samples. On the basis of these observations, it can be judged that the 255 °C phase transition must represent a transition between a low ordered LC phase (such as a N or smectic A or C phase) and I. This transition is close to thermodynamic equilibrium. Furthermore, these results indicate that even if PEFBP(n = 7) can be crystallized, its crystallization rate has to be very slow.

Figure 2a shows a schlieren texture observed in PLM after the PEFBP(n = 7) sample being isothermally kept at 120 °C for 12 h. Both two and four brushes of extinction (defect points) are seen, which is representative of the N phase. When the sample is heated to above 255 °C, this schlieren texture disappears and no birefringence can be observed. Therefore, the 255 °C transition is recognized as a N ↔ I transition. Figure 2b shows a banded texture induced by mechanical shearing. The bands are perpendicular to the shear direction and have a period of a few micrometers. Formation of these bands is due to slight relaxation of the molecules after shear-

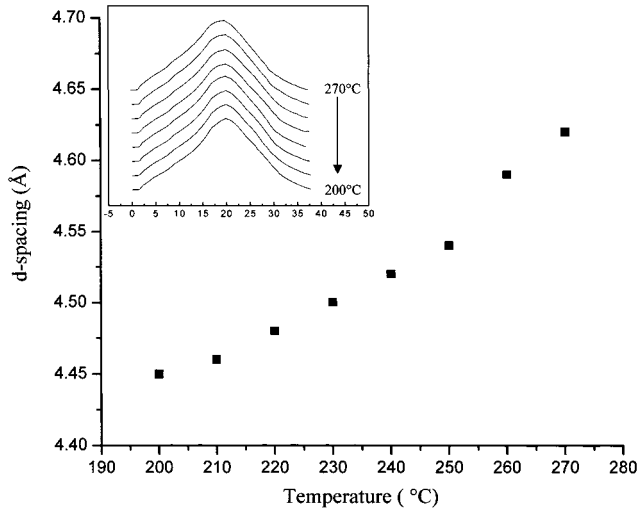

Figure 4. Relationship between the *d* spacing of the molecular lateral packing and temperature in the vicinity of the LC transition temperature region. The inset is a set of 1D WAXD patterns at different temperature in this transition region.

ing.[35,36] Note that the banded texture is usually not observed in sheared side-chain LCPs.

The existence of this N phase in PEFBP(n = 7) can also be evidenced by WAXD powder experiments as shown in Figure 3. In a temperature region between 50 and 270 °C, no low-angle and wide-angle Bragg reflections can be observed, indicating that neither long-range ordered layer structure nor laterally molecular packing exists in this sample. Careful examination leads to two overlapped scattering halos in a 2θ angle region of 2°−40°. This may suggest the existence of two short-range ordered periodicities. Deconvolution indicates that these two halos are centered at around 8° and 20° (see the inset of Figure 3). The scattering halo at 2θ of ∼20° (d-spacing of ∼0.42 nm) generally represents an average lateral distance among neighboring chain molecules. The origin of the scattering halo at 2θ of ∼8° (d spacing of ∼1.1 nm) is not yet clear at this moment. It might be attributed to the scattering of the side chains including 4-cyanobiphenyls, similar to small LC molecules. Yet, this halo has not been observed on the meridian in the WAXD fiber pattern due presumably to a very weak intensity. If we plot the d spacing of the 2θ of ∼20° halo vs temperature as shown in Figure 4, a sudden change of the d spacing is observed at ∼255 °C, and it is reversible during heating and cooling, revealing the N ↔ I phase transformation as reported in many other LCPs.[8,9,37−40]

Mesogens in LCPs are the components that are responsible for forming LC phases. The question is whether or not both the backbones and mesogens in the side chains of PEFBP(n = 7) are involved in constructing this N phase. It can be resolved by quantitatively evaluating the heat of transition of the N ↔ I. In the side-chain LC polyacrylate containing 4-cynobiphenyls, the heat of transition of the N ↔ I is 2.6 kJ/mol.[41] However, the side chains containing 4-cyanobiphenyls in PEFBP(n = 7) possess a weight percentage of 56%. Assuming that the N phase is only constructed by 4-cynaobiphenyls in the side chains, the heat of transition of this polymer should be 1.46 kJ/(mol of the PEFBP(n = 7) repeat unit) or 2.32 kJ/(mol of the 4-cyanobiphenyls). Compared with the experimentally observed value (2.78 kJ/mol), it is clear that the N phase in PEFBP(n = 7) is attributed to both of the 4-cyanobiphenyls in the side chains and the polyester backbones. The banded texture in Figure 2b also supports the conclusion.

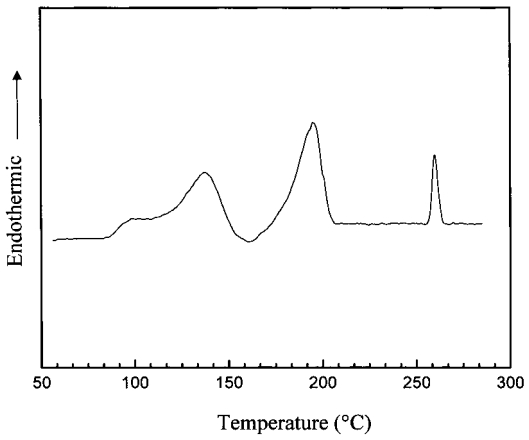

Figure 5. A DSC heating diagram for the oriented sample which was annealed at 100 °C for 12 h. The endothermic process at around 137 °C represents the melting of the SK_O phase.

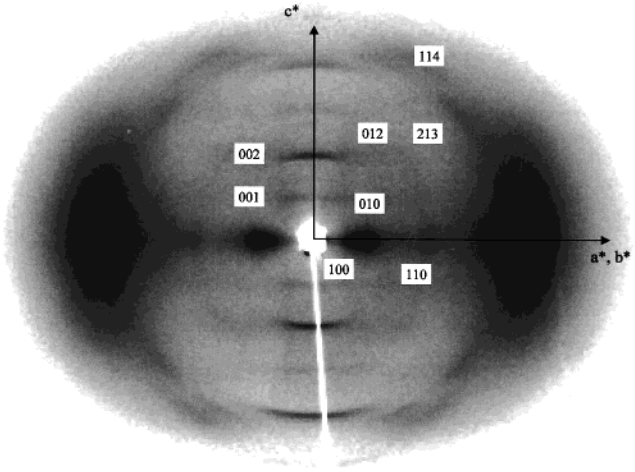

Figure 6. A WAXD fiber pattern of the SK_O phase in an oriented PEFBP(n = 7) sample.

Identification of the High-Ordered LC Phase. When the cooling rate is slower than 2.5 °C/min, a very small exothermic transition can be seen slightly above the T_g at ∼130 °C in DSC experiments. This transition is associated with a phase structure (the SK_O phase) of PEFBP(n = 7). In fact, when we anneal the sheared sample at 100 °C for 12 h, this phase can be further developed. Figure 5 shows a DSC heating diagram, which exhibits a clear endothermic process at ∼137 °C. This represents the SK_O phase meting. A recrystallization process follows, and this newly formed structure then melts at ∼195 °C (see below). For the SK_O phase, although its heat of transition increases continuously with prolonging t_c during the isothermal experiments, the transition temperature remains constant. The reason for this slow increase in heat of transition is due to the fact that the temperature of forming this SK_O phase is close to the T_g, and the slow transformation kinetics is caused by the hampered molecular motion (high viscosity).

The existence of this SK_O is confirmed by an oriented PEFBP(n = 7) WAXD fiber pattern as shown in Figure 6. The sample is annealed at 100 °C for 12 h. The layer spacing along the meridian of this pattern is observed

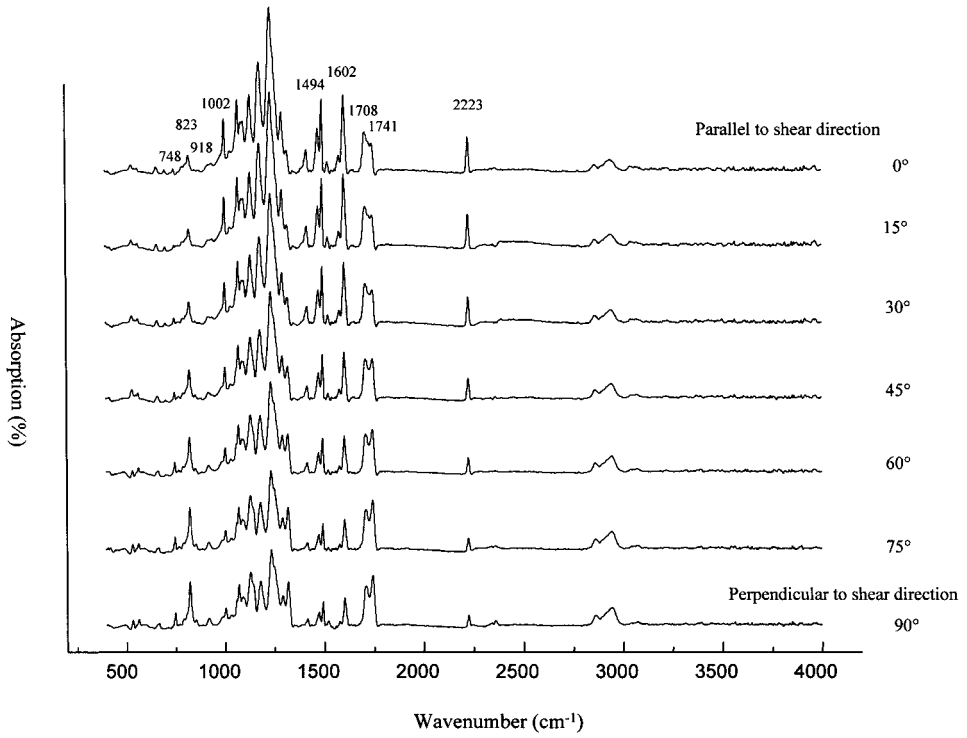

Figure 7. Set of polarized IR results at different rotating angles with respect to the orientation direction of the sample (from 0° to 90°).

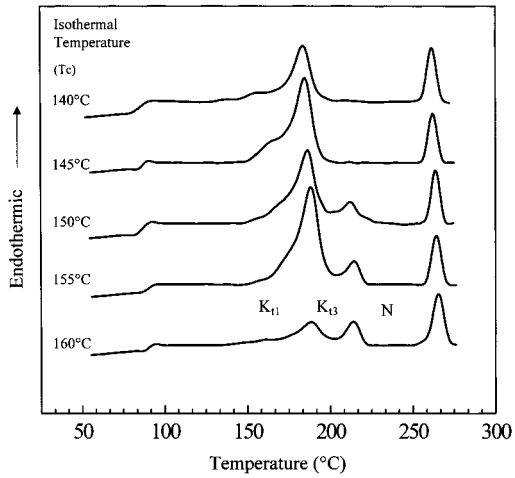

Figure 8. Set of DSC heating diagrams at 10 °C/min after the samples were isothermally crystallized at different temperature between 140 and 160 °C for 16 h.

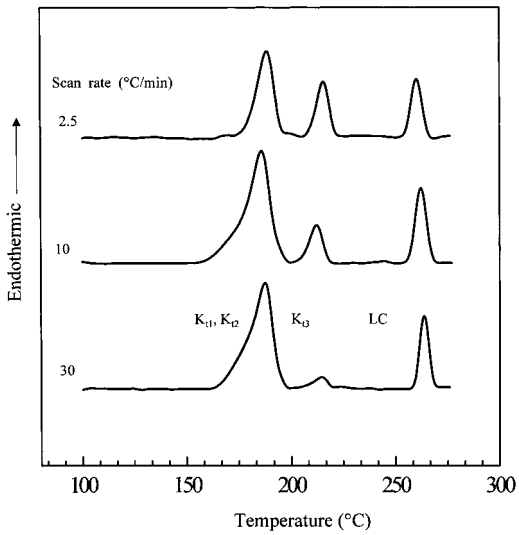

Figure 9. Set of DSC heating diagrams of PEFBP(n = 7) at different heating rates after the sample was isothermally crystallized at 155 °C for 16 h.

up to the fourth order with strong intensities of the even orders, indicating that along the meridian direction a long-range ordered layer structure exists. The *d*-spacing of the (002) diffraction on the meridian is comparative to the length of one repeat unit of the polyester backbone. On the equator of the fiber pattern, two diffractions are partially superposed at around $2\theta = 20°$, judged by the shape of the reflections. Several weak reflection pairs in the quadrants can also be observed. On the basis of these observations, the SK_O phase structure can be determined as an orthorhombic lattice having dimensions of $a = 1.55$ nm, $b = 0.98$ nm, and $c = 2.08$ nm and $\alpha = \beta = \gamma = 90°$. The weak intensities of the odd-order diffractions on the meridian can be explained by the extinction rule. This phase is similar to the orthorhombic lattice observed in other PEFBPs-(n = odd).[8,9]

One issue remaining is whether or not in the oriented PEFBP(n = 7) samples the orientation of 4-cyanobiphenyls in the side chains is parallel to the backbones along the orientation direction. Figure 7 shows the polarized IR experimental results of an oriented PEFBP(n = 7) sample at different rotating angles of the polarizer with respect to the orientation direction [recorded from 0° (parallel to the orientation direction) to 90° (perpendicular to the orientation direction) with an interval of 15°]. The CN stretching vibration band of the 4-cyanobiphenyls in the side chains at 2223 cm^{-1} continuously decreases in its intensity as the polarizer angle changes from 0° to 90°. The dichroic ratio ($A_{\parallel}/A_{\perp}$) of this CN stretching is 3.1, indicating that the dipole moment of this CN stretching vibration is parallel to the long axis of the 4-cyanobiphenyls. The vibration bands of the out-

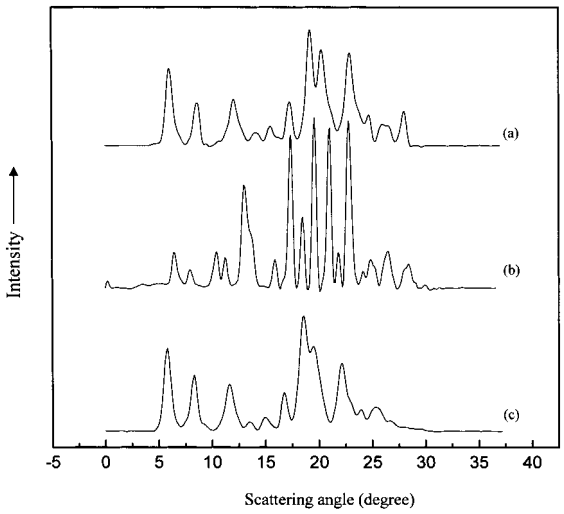

Figure 10. Three WAXD powder patterns after the samples were isothermally crystallized at 160 °C to form the K_{t1} phase (a), and the sample was further heated to 205 °C and annealed at that temperture for 36 h to form the K_{t3} phase (b), and the sample was quenched to 100 °C and then slowly heated to 150 °C and annealed at that temperature for 16 h to form the K_{t2} phase (c).

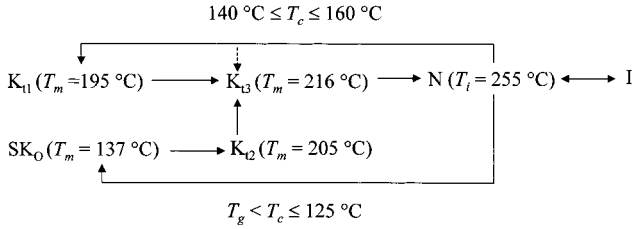

Figure 11. Phase transition sequence of the polymorphism in PEFBP(n = 7). The symbol of double arrow represents an equilibrium transition. The symbol of single arrow represents transformation of one phase to another. The symbol of broken single arrow represents a possible transition which needs prolonged t_c to develop.

of-plane CH bending of substituted phenylenes in both the backbones and side chains are at 748, 823, and 918 cm^{-1}. All three intensities increase as the polarizer rotates from 0° to 90°. Their $A_{\parallel}/A_{\perp}$'s are 0.33, 0.32, and 0.28, respectively. These out-of-plane bending vibrations have thus dipole moments which are perpendicular to the orientation direction. Meanwhile, the C−C stretching vibration bands in the phenylenes are at 1602 and 1494 cm^{-1}, and they show clear intensity decreases as the polarizer rotates from 0° to 90° (the $A_{\parallel}/A_{\perp}$'s are 3.1 and 3.0, respectively). Therefore, the dipole moments of these stretching vibrations are also parallel to the orientation direction. Furthermore, the backbone carbonyl stretching vibration band at 1741 cm^{-1} has the maximum intensity as the polarizer rotated to 90° with a $A_{\parallel}/A_{\perp}$ of 0.55, while the intensity of carbonyl stretching vibration in the side chains at 1708 cm^{-1} remains almost invariant during the rotation of polarizer. These results clearly demonstrate that the biphenyl groups in both of the backbones and the side chains are aligned in the orientation direction. The methylene units seem to be less oriented. Therefore, the orientation of backbones and side chains in the sheared PEFBP(n = 7) sample are parallel to each other and aligned with the orientation direction. When the orientated sample is heated to the crystals and the N phase, this orientation behavior is still kept. This also supports the conclusion based on the DSC and PLM observations that the backbones and mesogens in the side chains are cooperatively attributed to the construction of the N phase.

Identification of the Crystalline Phases. After the samples are completely crystallized at T_c's between 140 and 160 °C (usually after 10−40 h), multiple endothermic processes are found during heating at 10 °C/min as shown in Figure 8. The highest 255 °C temperature transition is attributed to the N ↔ I transition as previously determined. When $T_c \leq 145$ °C, only one transition can be observed at a peak temperature between 175 and 185 °C. (The lower temperature shoulder is a double melting phenomenon formed during the isothermal crystallization, and it is commonly found at about 10−15 °C higher than T_c.[42]) With increasing T_c, the main transition peak temperature slightly shifts to higher temperatures. However, when $T_c > 145$ °C, a separated, higher endothermic transition can also be seen at the peak temperature of ∼215 °C. With increasing T_c, this transition temperature also moves to higher temperatures. At $T_c = 160$ °C, the t_c of 16 h is not long enough to complete the crystallization and results in a low overall heat of crystal melting in Figure 8.

To understand interrelationships between these two transitions, Figure 9 shows a set of DSC heating diagrams with varying heating rates after the sample was crystallized at 155 °C for 16 h. With decreasing the heating rate, the heat of transition of the higher-temperature endothermic peak at ∼215 °C increases.

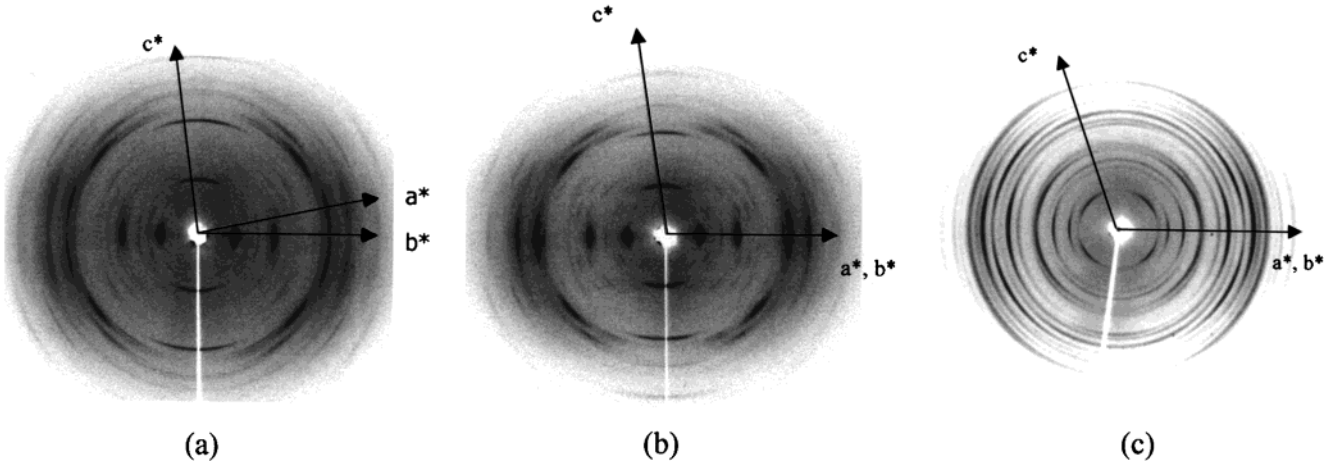

Figure 12. Three WAXD fiber patterns of the K_{t1} phase after the sample was annealed at 140 °C (a), the K_{t2} phase after the sample was quenched to 100 °C and then annealed at 150 °C (b), and the K_{t3} phase after the sample was annealed at 205 °C (c).

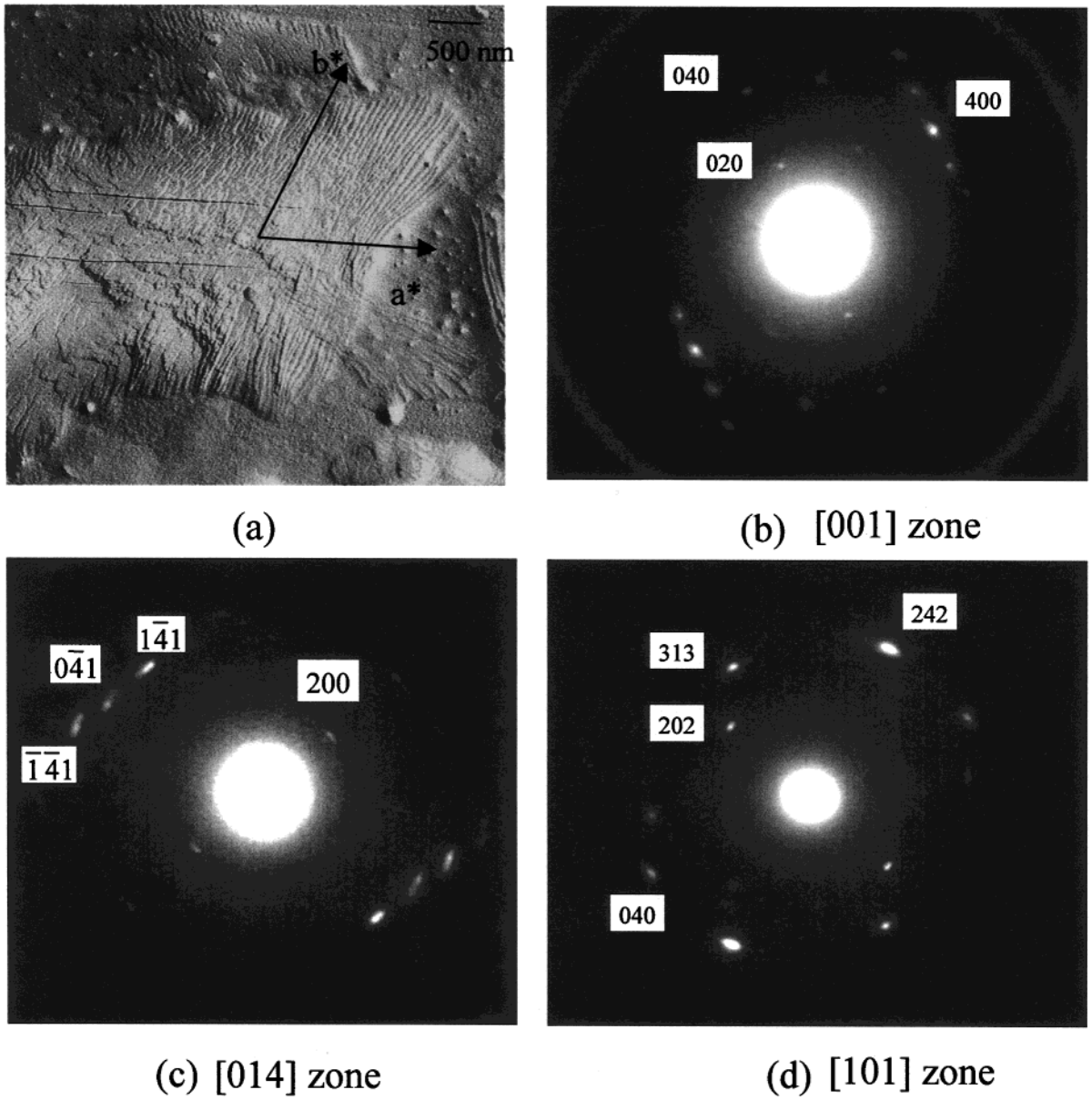

Figure 13. TEM morphology and SAED patterns for the K_{t1} phase. A bundle of the K_{t1} lamellar crystals (a), the [00*l*] zone ED pattern (b), the [014] zone ED pattern by 11° tilting the sample along the *a**-axis (c), and the [101] zone ED pattern by 40° tilting the sample along the *b**-axis (d).

This is an indication that a reorganization process takes place during heating. However, DSC experiments do not provide information on structural change associated with these thermal events. It is necessary to conduct WAXD experiments in order to know whether these two endothermic processes represent an identical crystal structure with different metastability or they actually possess different crystal structures.

Figure 10a shows the WAXD powder patterns on a sample which was annealed at 145 °C for 24 h after directly quenched from the N phase. We denote this phase as a K_{t1} phase. By slowly heating this sample to 205 °C and annealing at this temperature for $t_c = 36$ h, the WAXD powder pattern exhibits different diffraction angles and intensities (Figure 10b). This is assigned as the K_{t3} phase. It has also been found that this K_{t3} phase forms relatively fast as the sample is heated from the K_{t1} phase rather than the sample directly crystallizes from the N LC phase (several days are needed) due presumably to reorganization in forming primary nuclei of the K_{t3} phase from the K_{t1} phase during slow heating. However, another phase can also be formed via a pathway of slowly heating the sample from the SK_O phase to 150 °C and then annealed at that temperature. The WAXD powder pattern is shown in Figure 10c. Although this pattern is similar to the K_{t1} phase (compare parts a and c of Figure 10), analysis of the 2D WAXD fiber pattern of this phase indicates that the diffraction positions and intensities are substantially different from those of the K_{t1} phase. Therefore, this represents a new K_{t2} phase. This K_{t2} phase can also transfer to the K_{t3} phase during slow heating.

From these experimental observations, it is summarized that the K_{t1} phase is able to crystallize from the N phase. This K_{t1} phase can be transferred to the K_{t3} phase during heating. On the other hand, the K_{t2} phase is formed from the SK_O phase, and it can also be transferred to the K_{t3} phase during heating. However, we are unable to experimentally observe a transformation between the K_{t1} and K_{t2} phases. This may be due to either small difference of their thermodynamic stability or a high-energy barrier in transformation between

Table 1. Experimental and Calculated Crystallographic Parameters of the K_{t1} Triclinic Phase[a]

	2θ (deg)		d spacing (nm)		
(*hkl*)	expt	calc	expt	calc	int[b]
010	5.7	5.8	1.55	1.52	w
200	9.6	9.6	0.92	0.92	m
020	11.9	11.7	0.74	0.76	vs
300	14.3	14.4	0.62	0.61	w
140	24.5	24.9	0.36	0.36	vw
530	26.8	26.9	0.33	0.33	w
101	6.8	6.8	1.30	1.30	m
111	7.9	7.9	1.11	1.11	m
211	11.2	11.3	0.79	0.78	w
021	12.0	12.1	0.74	0.73	w
121	12.7	12.6	0.70	0.70	w
311	15.6	15.3	0.57	0.58	w
401	19.2	19.2	0.46	0.46	w
411	20.0	19.8	0.44	0.45	s
321	21.5	21.4	0.41	0.42	w
141	22.7	23.2	0.39	0.38	w
223	19.3	19.6	0.46	0.45	vs
033	20.5	20.9	0.43	0.43	m
014	18.6	18.6	0.48	0.48	w
504	28.0	28.0	0.32	0.32	w
002	8.5	8.5	1.03	1.03	vs
004	17.2	17.1	0.51	0.52	s

[a] The calculated data listed are based on the K_{t1} triclinic unit cell with $a = 1.89$ nm, $b = 1.57$ nm, $c = 2.09$ nm, $\alpha = 93.9°$, $\beta = 84.2°$, and $\gamma = 80.0°$. [b] The intensity are semiquantitatively estimated via a microdensitometer and classified as very strong (vs), strong (s), medium (m), weak (w), and very weak (vw).

Table 2. Experimental and Calculated Crystallographic Parameters of the K_{t2} Triclinic Phase[a]

	2θ (deg)		d spacing (nm)		
hkl	expt	calc	expt	calc	int[b]
010	5.8	5.9	1.52	1.50	vs
200	9.1	9.3	0.97	0.95	w
210	11.6	11.5	0.76	0.77	s
400	18.3	18.7	0.48	0.47	m
320	19.3	19.2	0.46	0.46	s
330	21.9	21.6	0.40	0.41	m
240	26.0	26.4	0.34	0.33	w
101	6.6	6.6	1.33	1.33	w
011	7.6	7.6	1.17	1.17	w
111	8.5	8.5	1.04	1.04	w
021	12.1	12.2	0.73	0.73	w
121	13.6	13.3	0.65	0.66	w
221	14.9	14.9	0.59	0.59	w
411	20.0	20.2	0.44	0.44	vw
112	11.5	11.2	0.77	0.79	w
122	15.3	15.3	0.58	0.58	w
422	23.9	23.7	0.37	0.38	w
213	18.4	18.3	0.48	0.49	s
413	23.9	23.8	0.37	0.37	w
114	19.7	19.8	0.45	0.45	w
014	17.9	17.7	0.49	0.50	vw
002	8.3	8.5	1.06	1.04	s

[a] The calculated data listed are based on the K_{t2} triclinic unit cell with $a = 1.91$ nm, $b = 1.52$ nm, $c = 2.07$ nm, $\alpha = 85.4°$, $\beta = 85.9°$, and $\gamma = 95.0°$. [b] The intensity are semiquantitatively estimated via a microdensitometer and classified as very strong (vs), strong (s), medium (m), weak (w), and very weak (vw).

these two phases.[43,44] A detailed phase transition sequence is illustrated in Figure 11.

Crystalline Structural Determinations. Parts a, b, and c of Figure 12 show three WAXD fiber patterns, which correspond to the K_{t1}, K_{t2}, and K_{t3} phases. These patterns exhibit obvious structural differences among them. For the K_{t1} and K_{t3} structures, the characteristic features of triclinic structure can be identified. In Figure 12a, the equator diffractions do not include (*hk*0) planes, and no diffractions can be found on the meridian. This implies that at least two of three reciprocal axes (*a**-, *b**-, or *c**-axis) are not on the equator and meridian. After the crystallographic analysis, it is found that only the *b**-axis is on the equator, while the *a**-axis is 12° tilted away from the equator. The *c**-axis is, on the other hand, 8° tilted away from the meridian. Therefore, only the (0*k*0) diffractions are on the equator, and the chain direction is not parallel to the fiber axis. Using the computer refinement, the K_{t1} crystal structure possesses a triclinic unit cell having dimensions of $a = 1.89$ nm, $b = 1.57$ nm, $c = 2.09$ nm, $\alpha = 93.9°$, $\beta = 84.2°$, and $\gamma = 80.0°$. The symmetry is $P\bar{1}$. The calculated crystallographic density for this four-chain cell is 1.33 g/cm^3, while the experimentally observed density is 1.32 g/cm^3. The calculated and experimentally observed 2θ and *d* spacing of diffractions are listed in Table 1. It needs to be pointed out that in this triclinic unit cell each motif possesses four chains, which is shared by neighboring four repeating units. Therefore, each triclinic cell possesses one motif.

This K_{t1} structural determination is also supported by the SAED results obtained in lamellar crystals. Figure 13a shows a bundle of lamellar crystals grown at $T_c = 158$ °C, and some twisting feature seems to exist: at the both ends of the lamellar bundle, the crystals are edge-on, while at the center they are more or less flat-on. Figure 13b shows the [00*l*] zone pattern at the center of the crystals. The (*hk*0) (where *h* and *k* = even) diffractions are brighter than others. When the sample is 11° or 40° tilted along the *a**- or *b**-axes, the [014] and [101] zone patterns can be observed (Figure 13, c and d, respectively). A 3D crystal unit cell can thus be constructed, and the result confirms the WAXD determined structure.

Table 3. Experimental and Calculated Crystallographic Parameters of the K_{t3} Triclinic Phase[a]

	2θ (deg)		d spacing (nm)		
hkl	expt	calc	expt	calc	int[b]
110	7.8	7.8	1.13	1.13	m
020	10.3	10.0	0.86	0.88	m
200	11.2	11.1	0.79	0.80	w
240	21.8	21.9	0.41	0.41	w
130	15.8	15.5	0.56	0.57	w
310	17.0	16.8	0.52	0.53	s
140	20.6	20.3	0.43	0.44	s
240	24.1	24.1	0.37	0.37	w
340	24.9	24.8	0.36	0.36	w
250	26.5	26.5	0.34	0.34	w
121	13.1	12.6	0.68	0.70	m
011	6.3	6.3	1.40	1.40	m
312	13.7	13.6	0.65	0.65	w
212	19.4	19.5	0.46	0.46	s
142	22.8	22.9	0.39	0.39	w
022	12.8	12.7	0.70	0.70	m
314	18.4	18.2	0.48	0.49	m
002	11.2	11.1	0.79	0.80	w

[a] The calculated data listed are based on the K_{t3} triclinic unit cell with $a = 1.96$ nm, $b = 1.93$ nm, $c = 2.03$ nm, $\alpha = 66.7°$, $\beta = 55.2°$, and $\gamma = 72.1°$. [b] The intensity are semiquantitatively estimated via a microdensitometer and classified as very strong (vs), strong (s), medium (m), weak (w), and very weak (vw).

For the K_{t2} WAXD fiber pattern in Figure 12b, diffractions are deviated from the meridian, indicating that the *c**-axis is not parallel to the fiber axis. On the other hand, both the (*h*00) and (0*k*0) diffractions are located on the equator. Detailed analysis shows that the K_{t2} phase possess a triclinic lattice with $a = 1.91$ nm, $b = 1.52$ nm, $c = 2.07$ nm, $\alpha = 85.4°$, $\beta = 85.9°$, and $\gamma =$

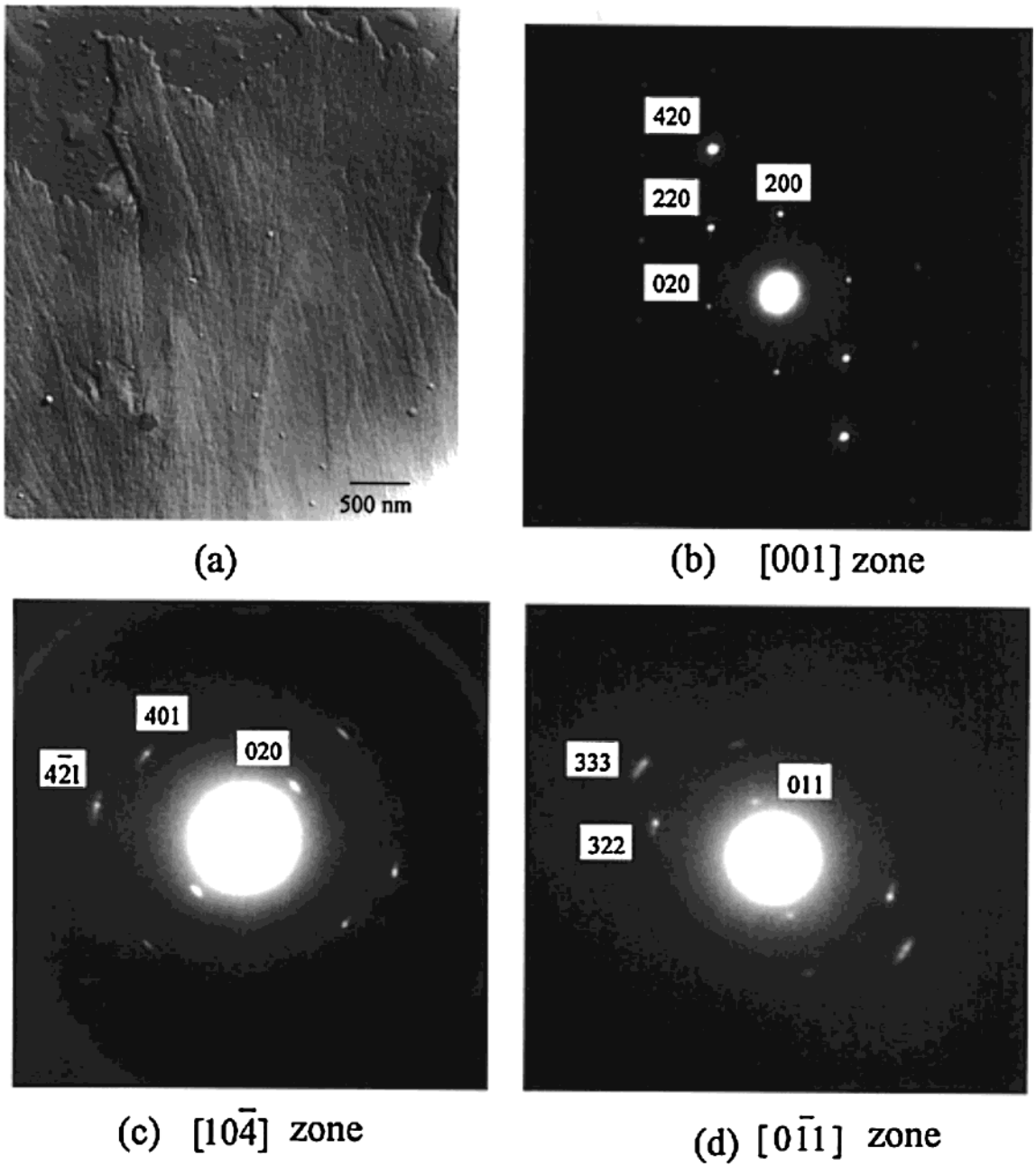

Figure 14. TEM morphology and SAED patterns for the K_{t3} phase. A flat K_{t3} lamellar crystal (a), the [00*l*] zone ED pattern (b), the [0$\bar{1}$1] zone ED pattern by 54° tilting the sample along the *a**-axis (c), and the [10$\bar{4}$] zone ED pattern by 12° tilting the sample along the *b**-axis (d).

95.0°. The symmetry is $P\bar{1}$. The *c**-axis is 12°-inclined with respect to the fiber axis. The calculated crystallographic density is 1.34 g/cm^3 for this four-chain cell. The calculated and experimentally observed 2θ and *d*-spacing of diffractions are listed in Table 2. It is evident that the unit-cell dimensions of the K_{t2} phase are significantly different from those of the K_{t1} phase. Disregarding our extensive efforts, growing K_{t2} lamellar single crystals has not been successful. Therefore, SAED results cannot be obtained.

To determine the K_{t3} structure (Figure 12c) is difficult due to a relatively poor crystal orientation. We can still manage to find that both the *a**- and *b**-axes are located on the equator, and the *c**-axis is tilted from the fiber axis. On the basis of the diffractions observed in Figure 12c, a triclinic unit cell can also be determined. The unit-cell dimensions are $a = 1.96$ nm, $b = 1.93$ nm, $c = 2.03$ nm, $\alpha = 66.7°$, $\beta = 55.2°$, and $\gamma = 72.1°$ after the refinement. The symmetry is $P\bar{1}$. The calculated crystal density is 1.38 g/cm^3 for this four-chain cell, compared with the experimentally observed density of 1.36 g/cm^3. The calculated and experimentally observed 2θ and *d* spacing of diffractions are listed in Table 3.

TEM morphology shows flat lamellar crystals of the K_{t3} phase (Figure 14a). Figure 14b−d is the SAED results which are the [00*l*], [0$\bar{1}$1], and [10$\bar{4}$] zone SAED patterns, respectively. For the latter two SAED patterns, the samples are 54° and 12° tilted along the *a**- and *b**-axes. Diffraction spots in these figures can be indexed on the basis of the determined triclinic structure, indicating that the SAED results support the WAXD determined K_{t3} structure.

Conclusion

In summary, the phase structures and transition behaviors of PEFBP($n = 7$) have been identified using

combined thermal (DSC), structural (WAXD, polarized IR and SAED), and morphological (PLM and TEM) methods. In addition to the low ordered N LC and the high ordered SK_O phases, three triclinic crystal (K_{t1}, K_{t2}, and K_{t3}) phases have been identified. Although these three triclinic structures have the identical symmetry, their unit-cell dimensions are different. The sequence of the phase transformations indicates that the K_{t3} phase is thermodynamically most stable phase, and the K_{t1} and K_{t2} phases are metastable with respect to the K_{t3} phase. They can be transferred to the K_{t3} phase during slow heating via reorganization and melting/recrystallization processes. The experimental access of these two metastable phases is due to the fact that the crystallization kinetics of the K_{t3} phase is extremely slow (namely, very high free energy barrier of the formation of this phase from the N phase). On the other hand, the formation kinetics of the K_{t1} and K_{t2} phases is relatively fast. It is surprising that the structural transformation between the K_{t1} and K_{t2} phases has not taken place. This may reflect the importance of the existence of the SK_O structure in forming the K_{t2} phase.

Acknowledgment. This work was supported by the NSF (DMR-96-17030) and the ALCOM Scientific and Technology Center (DMR-91-57738) at Kent State University, Case Western Reserve University, and the University of Akron.

References and Notes

(1) Balluauff, M.; Schmidt, G. F. *Makromol. Chem., Rapid Commun.* **1987**, *8*, 93.
(2) Berger, K.; Balluauff, M. *Mol. Cryst. Liq. Cryst.* **1987**, *147*, 163.
(3) Adam, A.; Spiess, W. *Makromol. Chem., Rapid Commun.* **1990**, *11*, 249.
(4) Frech, C. B.; Adam, A.; Falk, U.; Boeffel, C.; Spiess, W. *New Polym. Mater.* **1990**, *2*, 267.
(5) Cervinka, L.; Balluauff, M. *Colloid Polym. Sci.* **1992**, *270*, 859.
(6) Endres, B. W.; Ebert, M.; Wendorff, J. H.; Reck, B.; Ringdorf, H. *Liq. Cryst.* **1990**, *7*, 217.
(7) Ge, J. J.; Zhang, A.; McCreight, K. W.; Ho, R.-M.; Wang, S.-Y.; Jin, X.; Harris, F. W.; Cheng, S. Z. D. *Macromolecules* **1997**, *30*, 6498.
(8) Ge, J. J.; Honigfort, P. S.; Ho, R.-M.; Wang, S.-Y.; Harris, F. W.; Cheng, S. Z. D. *Macromol. Chem. Phys.* **1999**, *200*, 31.
(9) Chen, B.-Q.; Kameyama, A.; Nishikubo, T. *Macromolecules* **1999**, *32*, 6485.
(10) Reck, B.; Ringsdorf, H. *Makromol. Chem., Rapid Commun.* **1985**, *6*, 291.
(11) Reck, B.; Ringsdorf, H. *Makromol. Chem., Rapid Commun.* **1986**, *7*, 389.
(12) Voigt-Martin, I. G.; Durst, H.; Reck, B.; Ringsdorf, H. *Macromolecules* **1988**, *21*, 1620.
(13) Mensinger, H.; Biswas, A.; Poths, H. *Macromolecules* **1992**, *25*, 3156.
(14) Piao, X. L.; Kim, J.-S.; Yun, Y.-K.; Jin, J.-I.; Hong, S.-K. *Macromolecules* **1997**, *30*, 2294.
(15) Reck, B.; Ringsdorf, H. *Makromol. Chem.* **1989**, *190*, 2511.
(16) Kpitza, H.; Zentel, R. *Makromol. Chem.* **1991**, *192*, 1859.
(17) Pakula, T.; Zentel, R. *Makromol. Chem.* **1991**, *192*, 2401.
(18) Herrmann-Schonherr, O.; Wendorff, J.; Ringsdorf, H.; Tschirner, P. *Makromol. Chem., Rapid Commun.* **1987**, *7*, 791.
(19) Elbert, M.; Herrmann-Schonherr, O.; Wendorff, J.; Ringsdorf, H.; Tschirner, P. *Makromol. Chem., Rapid Commun.* **1988**, *9*, 445.
(20) Voigt-Martin, I. G.; Simon, P.; Bauer, S.; Ringsdorf, H. *Macromolecules* **1995**, *28*, 236.
(21) McCreight, K. W.; Ge, J. J.; Guo, M.; Mann, I.; Li, F.; Shen, Z.; Jin, X.; Harris, F. W.; Cheng, S. Z. D. *J. Polym. Sci., Polym. Phys. Ed.* **1999**, *7*, 1633.
(22) Kato, T.; Frechet, J. M. J. *Macromolecules* **1989**, *22*, 3818.
(23) Watanabe, J.; Harkeness, B. R.; Sone, M.; Ichimura, H. *Macromolecules* **1991**, *24*, 6759.
(24) Watanabe, J.; Harkeness, B. R.; Sone, M.; Ichimura, H. *Macromolecules* **1994**, *27*, 507.
(25) Ge, J. J.; Zhang, A.; McCreight, K. W.; Wang, S.-Y.; Jin, X.; Harris, F. W.; Cheng, S. Z. D. *Macromolecules* **1998**, *31*, 4093.
(26) Ge, J. J.; Guo, M.; Zhang, Z.; Honigfort, P. S.; Mann, I.; Wang, S.-Y.; Harris, F. W.; Cheng, S. Z. D. *Macromolecules* **2000**, *33*, 3983.
(27) Ge, J. J.; Zhang, J. Z.; Zhou, W.; Li, C. Y.; Jin, S.; Calhoun, B. H.; Wang, S.-Y.; Harris, F. W.; Cheng, S. Z. D. *J. Mater. Sci.* **2000**, *35*, 5215.
(28) Zentel, R. Conbined Liquid Crystalline Main-Chain/Side-Chain Polymers. In *Handbook of Liquid Crystals*; Demus, D., Goodby, J., Gray, G. W., Spiess, H. J.-W., Vill, V., Eds.; *High Molecular Weight Liquid Crystals*; Wiley-VCH: New York, 1998; Vol. 3, pp 52−65.
(29) Ge, J. J.; Xue, G.; Li, F.; McCreight, K. W.; Wang, S.-Y.; Harris, F. W.; Cheng, S. Z. D.; Shen, Y. R.; Zhuang, X. *Macromol. Rapid Commun.* **1998**, *19*, 619.
(30) Hong, S.-K.; Oh, M.; Zhuang, X.; Shen, Y. R.; Ge, J. J. Harris, F. W.; Cheng, S. Z. D. *Phys. Rev. E* **2001**, *63*, 051706−1.
(31) Ge, J. J.; Li, C. Y.; Xue, G.; Mann, I. K.; Zhang, D.; Wang, S.-Y.; Harris, F. W.; Cheng, S. Z. D.; Hong, E.-C.; Zhuang, X.; Shen, Y. R. *J. Am. Chem. Soc.* **2001**, *123*, 5768.
(32) Wang, S.-Y. Ph.D. Dissertation, Department of Polymer Science, The University of Akron, Akron, OH, 1995.
(33) Eashoo, M.; Wu, Z.; Zhang, A.; Shen, D.; Tse, C.; Harris, F. W.; Cheng, S. Z. D.; Garder, K. H.; Hsiao, B. S. *Macromol. Chem. Phys.* **1994**, *195*, 2207.
(34) Li, C. Y.; Wang, B.; Cheng, S. Z. D. X-ray analyses in polymers. In *Encyclopedia of Analytical Chemistry*; Meyers, R. A., Ed.; John Wiley & Sons: New York, 2000; pp 8105−8124.
(35) Ungar, G.; Feijoo, J. L.; Percec, V.; Tound, R. *Macromolecules* **1991**, *24*, 953.
(36) Yandrisits, M. A.; Cheng, S. Z. D.; Zhang, A.-Q.; Cheng, J.; Wunderlich, B.; Percec, V. *Macromolecules* **1992**, *25*, 2112.
(37) Pardey, R.; Zhang, A.; Gabori, P. A.; Harris, F. W.; Cheng, S. Z. D.; Adduci, J.; Facinelli, J. V.; Lenz, R. W. *Macromolecules* **1992**, *25*, 5060.
(38) Pardey, P.; Shen, D.; Gabori, P. A.; Harris, F. W.; Cheng, S. Z. D.; Adduci, J.; Facinelli, J. V.; Lenz, R. W. *Macromolecules* **1993**, *26*, 3687.
(39) Yoon, Y.; Zhang, A.; Ho, R.-M.; Cheng, S. Z. D.; Percec, V.; Chu, P. *Macromolecules* **1996**, *29*, 294.
(40) Yoon, Y.; Ho, R.-M.; Moon, B.-S.; Kim, D.; McCreight, K. W.; Li, F.; Harris, F. W.; Cheng, S. Z. D.; Percec, V.; Chu, P. *Macromolecules* **1996**, *29*, 3421.
(41) Shibaev, V. P.; Kostromin, S. G.; Plate, N. A. *Eur. Polym. J.* **1982**, *18*, 651.
(42) Cheng, S. Z. D.; Cao, M.; Wunderlich, B. *Macromolecules* **1986**, *19*, 1868.
(43) Keller, A.; Cheng, S. Z. D. *Polymer* **1998**, *39*, 4461.
(44) Cheng, S. Z. D.; Keller, A. *Annu. Rev. Mater. Sci.* **1998**, *28*, 533.

MA0115702